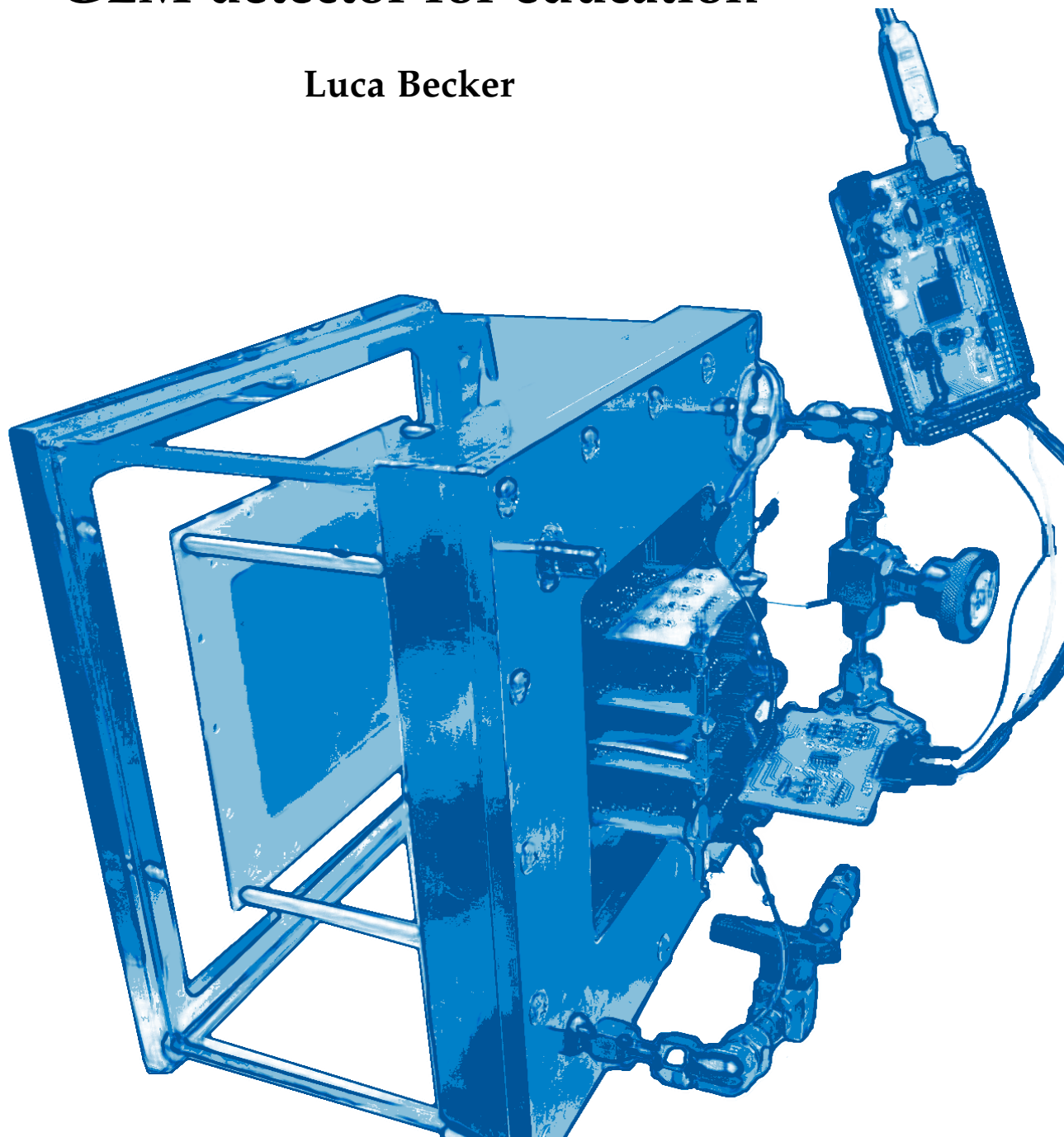
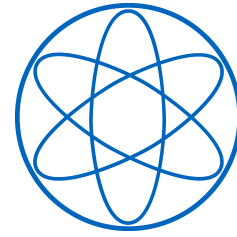
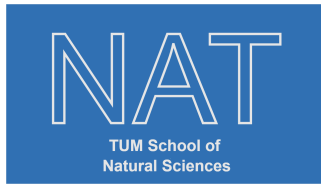


Bachelor's Thesis

Development of a multi-channel GEM detector for education

Luca Becker





Development of a multi-channel GEM detector for education

Entwicklung eines multi-channel GEM Detektors für Bildung

Dense and Strange Hadronic Matter E62

Bachelor's Thesis

Author: Luca Becker
Primary Reviewer: Prof. Dr. Laura Fabbietti
Supervisor: Berkin Ulukutlu
Date: October 18, 2024

I confirm that the results presented in this bachelor's thesis is my own work and I have documented all sources and materials used.

Ich versichere, dass ich diese Bachelorarbeit selbstständig verfasst und nur die angegebenen Quellen und Hilfsmittel verwendet habe.

Munich, October 18, 2024

Luca Becker

Abstract

High-energy physics stands at the frontier of knowledge, employing cutting-edge technologies to push the boundaries of our understanding through increasingly sophisticated measurement devices. These technologies are typically not available to the public; it is essential to provide young students with insights into cutting-edge experiments to foster their curiosity and interest in the modern sciences. The Origins Go-To School project aims to provide high school students with a learning experience that brings them closer to high-energy particle physics and the experiments carried out at CERN. As part of this experience, students will perform hands-on experiments on a detector based on state-of-the-art gaseous electron multiplier (GEM) technology. The detector is being developed at TUM and features off-the-shelf components for the readout electronics, which are not yet completely built. The detector incorporates 64 channels arranged in 8x8 pads and is planned to enable the live reconstruction of 2D images from cosmic particle tracks traversing the chamber.

This thesis details the design and production of a printed circuit board (PCB) that connects the front-end electronics to an Arduino microcontroller, which serves as the readout board. This interface was the last significant challenge in making the detector operational, primarily due to the slow processing speed of the Arduino. The existing electronics include an amplifier and a comparator, which measure the energy deposited by incoming charged particles using a time-over-threshold method and produce a square-wave output signal. The circuitry developed in this thesis converts this signal into a voltage stored in a capacitor, ready for readout by the Arduino, and allows for automatic resetting of the capacitor after the successful completion of the readout command. This approach addresses the limitations of the Arduino's slow readout speed. The circuit has been first tested and characterised using single-channel prototypes and meets all the requirements placed on it. With this, a multi-channel readout card featuring a multiplexer was designed, produced, and tested via pulsing to be used for the final outreach detector. Additionally, the thesis also explains the underlying principles and physical phenomena relevant to the operation of the outreach GEM detector and the electronics integrated into the developed PCB. The theory will in part be employed during the teaching of students via a dedicated manual which is also prepared.

Contents

1	Introduction	1
1.1	High energy physics in education	1
1.2	Use of detectors in demonstration	1
1.2.1	CERN Minipix	1
1.2.2	MuonPi	2
1.2.3	Origins Go-To School	2
2	GEM based demonstrator	4
2.1	Detector design & Working principle	4
2.1.1	Ionization	5
2.1.2	Recombination	6
2.1.3	Drift field	6
2.1.4	Theory of electron drift and diffusion	7
2.1.5	Gas properties in electrical fields	8
2.1.6	GEM foil	12
2.1.7	Particle identification	13
2.2	Readout System	14
2.2.1	Negative Gain Amplifier	15
2.2.2	Comparator	16
2.2.3	Interlude	17
2.2.4	ToT signal to voltage converter	18
2.3	Performance	26
3	Summary, Conclusion and Outlook	30
3.1	Summary	30
3.2	Conclusion	31
3.3	Outlook	31
4	Appendix	33
	List of Figures	38
	List of Tables	40
	Bibliography	41

1 Introduction

TUM has partnerships with many schools throughout Bavaria and offers interesting projects for young students. On my first day at university, I was still a pupil myself when my class was invited to a gene laboratory to solve a thrilling murder case. From that day on, I knew what I wanted to study. This work is part of a larger project aimed at getting the new generation interested in natural sciences and introducing them to high-energy particle physics through a hands-on experiment.

1.1 High energy physics in education

The Large Hadron Collider (LHC) at the European Organization for Nuclear Research (CERN) has a diameter close to 27 km and is packed with 9300 magnets, cooled to a freezing 1.9 K. Teachers would be hard pressed to recreate these conditions in a classroom. But we can't do without experiments either, as they are indispensable for the knowledge acquisition competence area of the educational standards (Erkenntnisgewinnungskompetenz der Bildungsstandards, KMK2020 [1]). So teachers often resort to simulations or simplified experimental set-ups. When using simulations, students cannot learn process-related skills for experimentation, so experiments are often preferred.

1.2 Use of detectors in demonstration

The German electron synchrotron (DESY) published a handbook, funded by the Federal Ministry of Education and Research, for self-construction of a cloud chamber. A cloud chamber is a simple detector that can be used to visualize tracks of particles flying through it. While they were used to make spectacular discoveries in the 1930s, today they can be found in museums and scientific exhibitions [2]. This project is an effort to bring modern detector techniques into the classroom.

1.2.1 CERN Minipix

The efforts of the detector experts at CERN themselves have already shown award winning results [3]. Detectors of the Minipix series, an example shown in figure 1.1, are silicon based pixel detectors. A grid of semiconductor elements measure charges deposited by particles. Each element is a pixel connected to its own read-out electronics channel. The resulting image displays background radiation in real time and can be used to broadly categorize different particles [4]. The MiniPIX EDU is a model designed for physics classes and features 256 by 256 pixels.

1 Introduction



Figure 1.1: Picture of the CERN Minipix detector. [5]

The Minipix detector is the size of an USB stick and just like an USB stick, it can be plugged into any computer and start visualizing background radiation. Its compact size and simple operation are also a crux when it comes to teaching. The standing conference of the ministers of education and cultural Affairs (KMK) emphasizes the importance for planning experiments and understanding the experimental setup (KMK 2020, [6, 7]). The Minipix's operation and inner structure are obscure for students and can not be examined.

1.2.2 MuonPi

The MuonPi is a detector specializing in the detection of muons, developed at the physics institute of the Justus-Liebig-university in Gießen, Germany. Muons are usually discussed in schools in the context of special relativity and cosmic radiation. A muon shower can be initiated by high energy cosmic particles in the outer atmosphere. Data collected by all MuonPi devices can be seen on a live map [8]. The project's mission is to study these cosmic showers by building an extensive network of low-cost particle detectors based on the RaspberryPi platform and distributing them across Europe. The hope is to identify a cosmic shower by tracking coincidences across different devices, even though most coincidences are random. The project tries to correlate these showers with atmospheric conditions like thunderstorms [9]. Unfortunately a MuonPi will most likely have to be self-assembled, which can be a high hurdle [10]. But even then the rather complex UI makes it difficult for pupils to operate the device.

1.2.3 Origins Go-To School

The aim of this project is to create a comprehensive learning environment for physics students to learn the concepts necessary to gain hands-on experience with a detector that operates on the same principles as the state-of-the-art detectors used in the ALICE experiment. Students will playfully explore the design of the detector using a Lego model (shown in figure 1.2 [11] and accompanying AR software.

Regarding the teaching format, students will first get to hear a lecture by a professor concerning some fundamental concepts to allow an equal playing field for all students regardless of the level of prior knowledge that different students might have. Here

1 Introduction

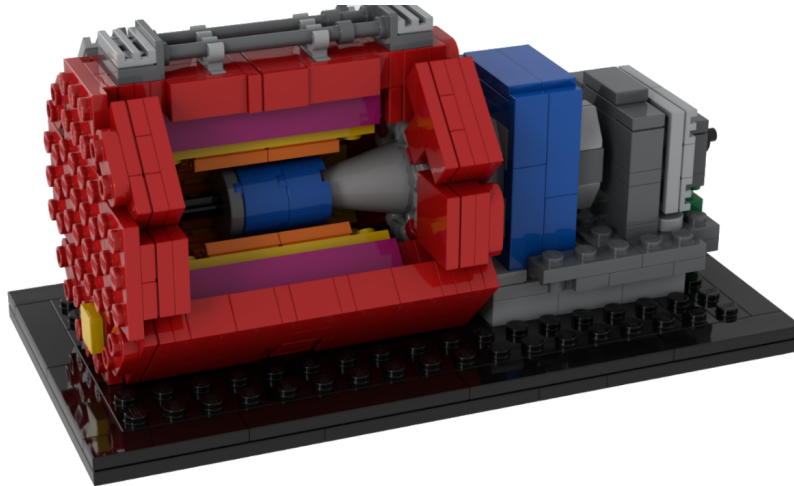


Figure 1.2: Photo of the Lego model, to be built by the students to learn the different detector systems of the ALICE experiment.

they will learn about anti-matter and annihilation with matter, how we came to learn about dark matter from observing rotation curves and theories about what dark matter might be made of, especially about weakly interacting massive particles (WIMPs) and that they might decay via weak interactions into massive anti-matter particles. The final fundamental concept - cosmic rays - smoothly leads to the question how all these kinds of particles might be measured. With a Lego model of the ALICE detector in hand and AR goggles on their head, they get to explore the structure and functionality of different components of the ALICE detector, that they have just pieced together themselves in the Lego model. With a basic conception of the ALICE detector in the forefront of their mind, they get to put their hands on a portable detector working on the very same principles they have just learned about. Operating the detector themselves they get to measure tracks of background radiation in real time. Going back to the ALICE detector they get to put everything they have learned together: The creation of matter-antimatter pairs from collisions at the LHC gives a probability for creating anti-Helium 3 in collisions. This allows to calculate how many anti-Helium cores we might expect to measure in outer space. A possible discrepancy between the expected value from events with cosmic rays and measurements performed on the ISS for the real saturation of anti-Helium in the cosmos might hint at the nature of dark matter as a weakly interacting massive particle capable of decaying into matter-antimatter pairs. As a part of the thesis a document has been written, explaining the GEM detector used for the science outreach project on a level appropriate for the students and drawing parallels to the detector used in the ALICE experiment. In this thesis, the development of the multi-channel read-out electronics for a gaseous electron multiplier detector are presented. A circuit diagram for the electronics are designed and based on this design, a printed circuit board (PCB) is developed, produced and tested.

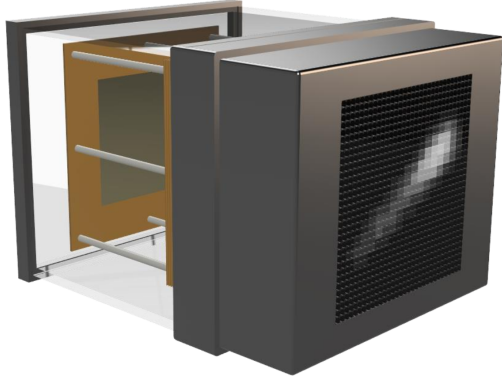
2 GEM based demonstrator

Gas electron multipliers (GEMs) are gaseous detectors used in CMS (Compact Muon Solenoid) and ALICE (A large hadron collider experiment) at CERN for their high rate capabilities and ability to resist high radiation doses [12]. GEMs are a more advanced iteration of the Multiwire Proportional Chamber (MWPC), designed 1968 by Georges Charpak. Detectors of this kind are called Micro-Pattern Gas Detectors (MPDGs). The following chapter concerns the GEM designed for the outreach project.

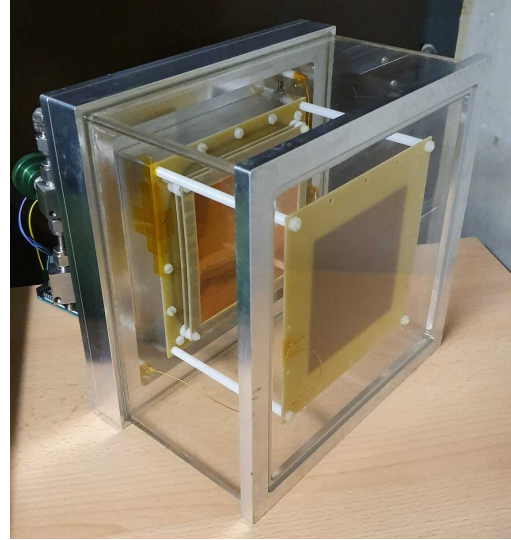
2.1 Detector design & Working principle

The general shape of the detector as shown in figure 2.1a is a 16 cm wide glass and aluminum box with a front surface of 24 cm by 24 cm, which is sealed and filled with an Argon-CO₂ gas mixture. Being able to see inside the detector improves demonstration purposes by allowing to directly point at different components and observing discharges on the GEM foils. A cathode and an anode are situated on opposing faces of the chamber. At the 10 cmx10 cm Anode there are 64 copper pads in a 8 by 8 grid, each 12.5 mmx12.5 mm in size, for signal detection. This layout allows for a Cartesian two-dimensional readout. The vital-piece of the detector is the GEM electrode. The GEM electrode, produced at the CERN PCB workshop with the double-mask technology, is of standard design: 50 μm thick polyimide (Apical) covered on both sides with 5 μm layers of copper, with 50 μm (70 μm) inner (outer) hole diameter and a pitch of 140 μm . A similar foil can be seen in figure 2.6a, which shows a photo of a GEM foil taken by an electron microscope.

A stack of two GEM electrodes is situated just above the copper pads. The gaps between the anode and the consecutive GEM foils is set to 4 mm and the drift gap between the top GEM foil and the cathode electrode is 10 cm, leading to a relatively large active volume increasing the rate of cosmic tracks expected to be measured up to 3 Hz.



(a) Render of the to-be-produced GEM-based detector with a built-in monitor displaying live measurements of tracks.



(b) Photo of the assembled outreach chamber.

Figure 2.1: GEM Detector Render and Outreach Chamber Photo

A single channel power coupled with a resistor chain voltage divider applies different potentials to cathode, top and bottom faces of each GEM, and anode (set to ground potential). This results in a 340.6 V/cm drift field between cathode and the top of the first GEM, a 2340.43 V/cm and 2246.81 V/cm field within the first and second GEM electrode respectively, a 468.09 V/cm transfer field between the GEMs and finally an induction field between the bottom layer of the second GEM and the anode.

2.1.1 Ionization

When a fast particle moves through the gas in our detector, it leads to the excitation of the gas particles. For energy transfers above a threshold value, the gas can also get ionized. This leads to the creation of a pair of an ion and a free electron, known as primary ionization. The applied electric field in the active field overpowers the Coulomb attraction between the positively charged ion and the negative electron (which, without a sufficiently strong field, leads to the recombination, see subchapter below), causing them to drift apart. During the drift process, if the electron gains sufficient energy from the applied field, it may lead to the creation of additional ion-electron pairs until the energy of the electron is below the ionization threshold. This is known as secondary ionization. The energy loss of an ionizing particle with energy E , charge z , and speed v per distance x traveled through a medium with electron density n and mean excitation energy I is described by the Bethe-Bloch formula. The relativistic form is:

$$-\frac{dE}{dx} = \frac{4\pi n z^2}{m_e c^2 \beta^2} \cdot \left(\frac{e^2}{4\pi\epsilon_0} \right)^2 \cdot \left[\ln \left(\frac{2m_e c^2 \beta^2}{I \cdot (1 - \beta^2)} \right) - \beta^2 \right] \quad (2.1)$$

Where m_e is the electron rest mass, c the speed of light, $\beta = \frac{v}{c}$ and e the elementary charge. Since the detector is meant for demonstration purposes and will be used to measure cosmic particles or radioactive decay, we can expect an energy transfer of several keV/cm. Argon and CO₂, a mix of which fills the detector, have a first ionization energy of 21.6 eV and 13.7 eV respectively. Naively dividing the deposited energy by the mean ionization energy, we might expect about 200 electrons to be released per centimeter from a particle depositing 3 keV/cm. Measurements, however, reveal about 100 ion-electron pairs for such a particle with only small variation from the type of particle or gas [13]. This is because low energy transfers are more probable, and with the energy threshold requirement for ionization, the process is dominated by excitation reactions.

2.1.2 Recombination

In the absence of a sufficiently strong electrical field electrons recombine with ions under the force of their electrical attraction. Recombination can happen via multiple reactions, in our case most importantly via emission recombination. During the slow process of emission recombination, the electron recombines with the ion (X as a variable for either Ar or CO₂), emitting a photon ($h\nu$).



2.1.3 Drift field

Applying a potential difference to the cathode and anode generates an electrical field across the detector. A Coulomb force of equal magnitude but in the opposite direction acts on the free electron and the ion. Recombination may still occur if the field strength is low and the Coulomb force can not fully negate the attraction between the ion-electron pair. Increasing the voltage between anode and cathode reduces the chance of recombination. This behaviour is displayed in the first region of figure 2.2. The figure shows the number of ions collected versus applied voltage. It is not the exact numbers in the figure that are important, but the behaviour of the curve in the different areas. Beyond the first region all recombination is halted and further increases in voltage can not lead to a higher yield, as represented by the flat line in region II of the figure. Operating the detector with a field in the second region separates the ions and electrons, transferring them towards cathode and anode respectively. The electrons will eventually be amplified and measured on the anode as a current. This separation of electron amplification and signal induction into different regions of the detector is a key advantage of GEM detectors over traditional gas detectors, as it allows for quick evacuation of the ions. This has two effects. On the one hand it is preventing gas discharges and is thus protecting the sensitive read-out electronics. On the other hand it allows GEMs to reach a higher rate capability [14]).

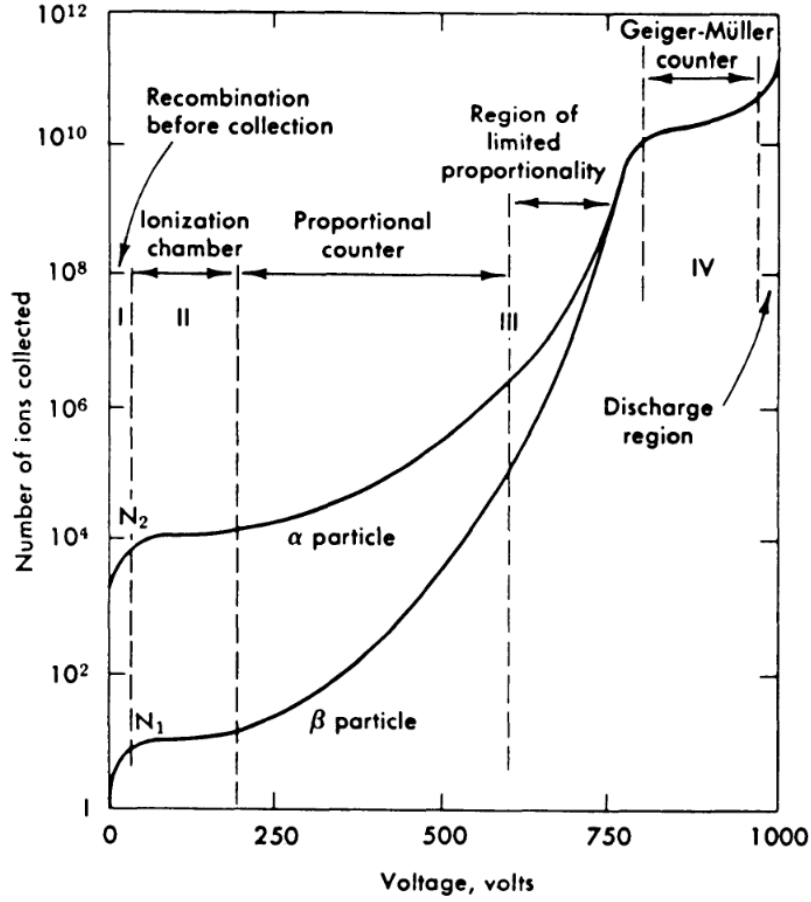


Figure 2.2: Number of ions collected versus the voltage for a singular wire ionization detector for α and β particles. [15]

2.1.4 Theory of electron drift and diffusion

The position of the ionized electrons is to be measured in order to reconstruct the ionizing particles trajectory. Therefore it is important to discuss the electron's motion through the gas and electrical field. Without external forces, charges with mass m in an ideal gas with temperature T move in random directions with different velocities. Their movement is described by the Maxwell-Boltzmann distribution, giving this

$$p(v) = 4\pi \left(\frac{m}{2\pi k_B T} \right)^{3/2} v^2 \exp \left(-\frac{mv^2}{2k_B T} \right) \quad (2.3)$$

normal distribution for the particle's velocity v with a standard deviation of $\sigma = \sqrt{\frac{k_B T}{m}}$, where k_B is the Boltzmann constant. Integration gives a mean velocity

$$\bar{v} = \int_0^\infty v p(v) dv = \sqrt{\frac{8k_B T}{\pi m}} \quad (2.4)$$

which results in about 10^5 m/s for an electron at room temperature. Adding an external E field accelerates ions and electrons toward cathode and anode respectively along the

2 GEM based demonstrator

field lines. Collisions with gas particles limit the charge's velocity to an average drift velocity

$$w = \frac{eE}{m} \left\langle \frac{l}{v} \right\rangle = \frac{eE}{m} \tau \quad (2.5)$$

which depends on the mean free path length l or alternatively the average time between collisions τ . The mean free time at constant pressure is considered constant, while the drift velocity increases linearly with the electric field. The mean free path l is inversely proportional to the gas pressure P . In an electric field the electron's temperature, and thus its energy and velocity are a function of the reduced electric field E/P . This affects the charge's motion previously described by the Maxwell-Boltzmann distribution. The standard deviation in a direction x is now better described as

$$\sigma_x = \sqrt{\frac{2Dx}{w}}, \quad (2.6)$$

with a field-dependent diffusion coefficient D . The Nernst-Einstein relation

$$D = \frac{\mu k_B T}{e} \quad (2.7)$$

links the diffusion coefficient D with the mobility of a charge $\mu = w/E$. Substitution in Eq. 2.6 gives

$$\sigma_x = \sqrt{\frac{2k_B T x}{eE}}, \quad (2.8)$$

the thermal limit to electron diffusion [16]). If mean energies of the electrons exceed thermal energies, the factor $k_B T$ in Eq. 2.7 is to be replaced by that mean energy. The diffusion constant D increases with the applied drift field E , strengthening diffusion and harming the resolution of the detector. The limit value for thermal energies differs greatly with different gases. CO₂ is considered a cool gas, the thermal approximation remains accurate even for high electron energies. The electron energy in Argon gas, however, becomes critical at a few V/cm atm. The high electron energy shortens time between collisions, so high field strengths would quickly result in gas discharges. From Eq. 2.7 one would expect resolution to improve with lower drift velocity. However, empirical data show that the resolution is worse in a 95/5 Ar/CO₂ mixture with a lower drift velocity than in a 50/50 argon/ethane mixture at the same gas pressures and the same electric field. [16] Clearly properties of the specific gas can not be neglected.

2.1.5 Gas properties in electrical fields

To properly explain electron transport, detector resolutions and the later discussed gains during electron amplification, properties of the involved gases need to be discussed. For electron transport the Ramsauer-Townsend effect is important. Using classical mechanics one would assume slow electrons to suffer greater deflections from the electrical field inside the atoms. So the cross section for scattering should be lower for electrons with higher kinetic energies. Ramsauer, however, found optimal permeability of electrons with energies around 1 eV. This phenomenon is commonly explained with de Broglie's theory of matter waves. For a high scattering cross section the electron's

de Broglie wavelength needs to be of the same order as the size of the gas atom. So the longer wavelength of slower electrons allows for better transport through the gas.

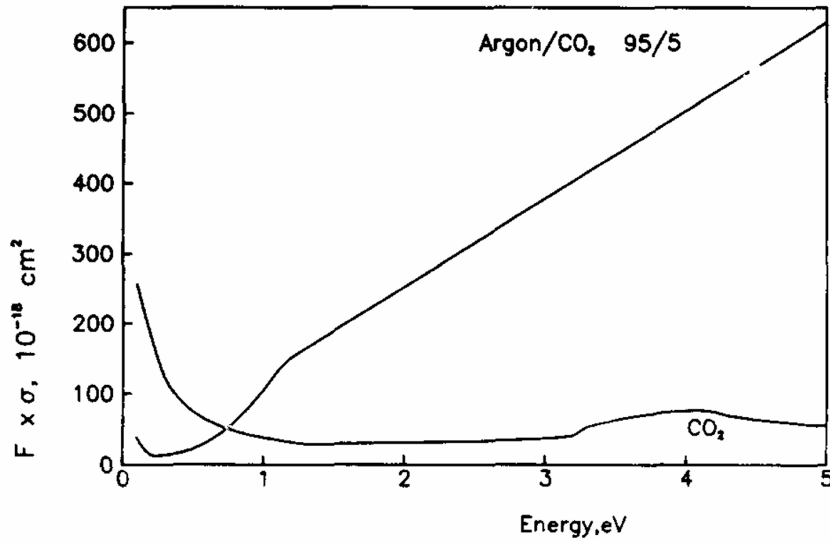
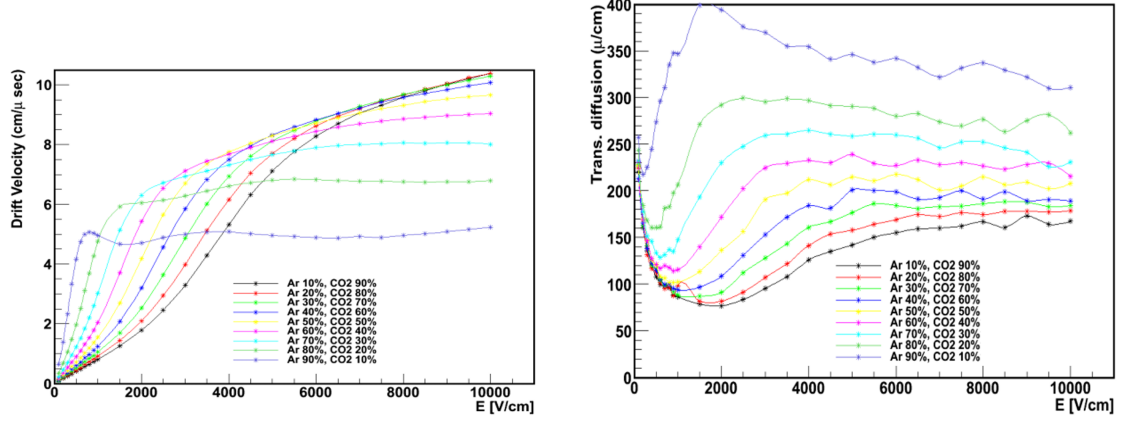


Figure 2.3: Product of momentum transfer cross section and fractional concentration by volume, F , versus electron energy for pure CO_2 and a 95/5 argon/ CO_2 gas mixture. Elastic scatters on argon dominate at higher energies. The Ramsauer minimum can be seen. [16]

Figure 2.3 shows the high transparency of an argon/ CO_2 mixture compared to pure CO_2 for low energies like our drift field or transfer field. Figure 2.4a shows drift velocities of varying argon/ CO_2 mixtures. From our conclusions from Eq. 2.7 we would expect the 10/90 Ar/ CO_2 mixture with its lowest drift velocity to support the best resolution. Indeed, figure 2.4b shows that this ratio has the lowest transversal diffusion. It even has the lowest longitudinal diffusion, but as that is only important for time projection - something our detector is not capable of - further analysis of longitudinal diffusion is excluded.



(a) Drift velocities of Ar/CO₂ mixtures for different percentages. Higher CO₂ concentration results in lower velocity for all operating voltages. [17]

(b) Transversal diffusion of Ar/CO₂ mixtures for different percentages. Higher CO₂ concentration results in lower diffusion for all operating voltages. [17]

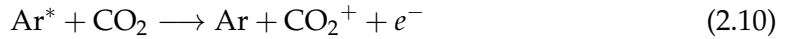
Figure 2.4: Drift Velocity and Transversal Diffusion of Ar/CO₂ Mixtures

Inelastic collisions in CO₂, due to their lower energy transfer, reduce the mean free path. This explains the lower drift velocity for higher CO₂ concentrations.

Let us now discuss the behaviour at higher fields, where ionization can occur. The most direct channel is for an electron to impact an atom, knocking an electron free and leaving the atom ionized:



The process is fittingly named impact ionization. Once again X is a stand-in for either Ar or CO₂. Ionization can also occur indirectly. Instead of ionizing, the accelerated electron might only excite its collision partner. Particularly in the case of argon this might yet result in ionization. How this might happen becomes apparent when studying the energy levels of argon, shown in table 2.1. Some excitation energy levels exceed 13.7 eV, the ionization energy of CO₂. Collisions of the excited atoms with a CO₂ molecule can then release further electrons in a process called Penning transfer:



Due to Penning transfers more ion-electron pairs are produced in total, making significant contribution to the gas gain curve. The effect is named after Frans Michel Penning who noticed a higher discharge potential in pure noble gases than in mixtures.

A more problematic channel for electron production happens when excited argon atoms fall back to their ground state with the emission of a UV photon:



Such photons, if not absorbed by the CO₂ gas, can release electrons from the cathode surface, or if they carry sufficient energy may ionize CO₂ molecules. Electrons produced in that way are separated from the avalanche and may produce their own avalanche, changing the gas gain curve to be over-exponential, called photon feedback. [19]

2 GEM based demonstrator

Excited levels of argon atom		
Term	Excitation energy [eV]	Remarks
1S_0	0	Fundamental State
3P_2	11.545	Metastable level
3P_1	11.620	Resonance level
3P_0	11.720	Metastable level
1P_1	11.825	Resonance level
$^1,^3S, P, D$	12.7-13.3	
$^1,^3P$	14.0-14.9	
$^1,^3P, D, F$	14.1-14.3	
	15.68	Ionisation
	15.87	

Table 2.1: Energy levels of Argon [18].

Instead of amplifying the electron avalanche, a phenomenon called electron capture or attachment, can remove electrons from the equation. A free electron can become attached to the electronegative CO_2 . The resulting CO_2^- anion has lower energy than its ground state and is thus stable, resulting in the loss of the electron. Because of the release of energy, called electron affinity, electron attachment requires the presence of a third particle to dissipate that energy. Another channel by which an electron may be lost is

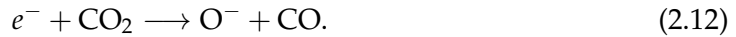


Figure 2.5 shows the loss/cm by attachment, the attachment coefficient, for a given field strength. Losses due to attachment are fortunately irrelevant in the drift field, but are unavoidable at higher fields necessary for electron multiplication.

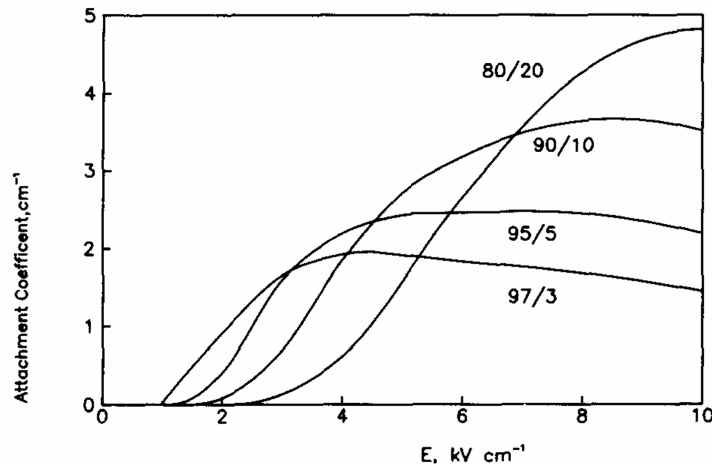


Figure 2.5: Electron attachment coefficients as a function of field E for various Ar/ CO_2 mixtures at 1 bar. The process considered is 2.12 [16]

In conclusion, argon is used for its high drift velocity, electron mobility and transparency, allowing for swift collection of charges and high gas gains. Being a 'warm'

gas, meaning average electron energies exceed the thermal limit, pure argon gas has high diffusion and easily leads to discharges. To balance this, a 'cool' quencher gas like Methane, Ethane, dimethylether (DME) or in our case carbon dioxide is introduced. This reduces diffusion while keeping a high drift velocity and by absorbing UV photons emitted by excited argon atoms prevents runaway avalanches and thus discharges at operating fields.

2.1.6 GEM foil

So far we have followed the detector's functionality from the moment a particle passing through the detector, to the ionization of the gas and how the released electrons behave in the gas under the influences of an electrical field and how they drift towards the anode to be measured as a signal. A current induced by only a hundred or so electrons from the primary ionization event would be too difficult to measure, so the signal needs to be amplified first. The theory of electron avalanches has been established, but the question of how these avalanches are created in our detector remains. This is where the aforementioned vital-piece, the GEM electrode, of the detector comes into play. By applying a voltage to the top and bottom of a GEM foil, a strong electrical field is generated in the holes. As seen in figure 2.6b, the field is strongest and quite uniform within the holes. Outside, the field falls off quickly, resulting in a concentrated multiplication volume separated from the rest of the drift chamber. The effects of high electrical fields on electrons results in electron avalanches as described above, effectively multiplying incoming electrons by a factor depending on the applied field strength. Unfortunately the multiplication factor can not be increased indefinitely. Eventually the large amount of ionization created through multiplication distorts the electrical field, leading to the region of limited proportionality in figure 2.2. When the field strength is increased further the quenching gas can not keep up and photon feedback results in a chain reaction of unwanted avalanches until discharge occurs. This fourth region is named after the Geiger-Müller counter operating in this region. Beyond that lies the discharge region. The accompanying continuous discharge is harmful to the equipment. [13]. A single GEM electrode can reach effective gains of up to ten thousand, although a gain below one thousand is recommended for safer operation [20].

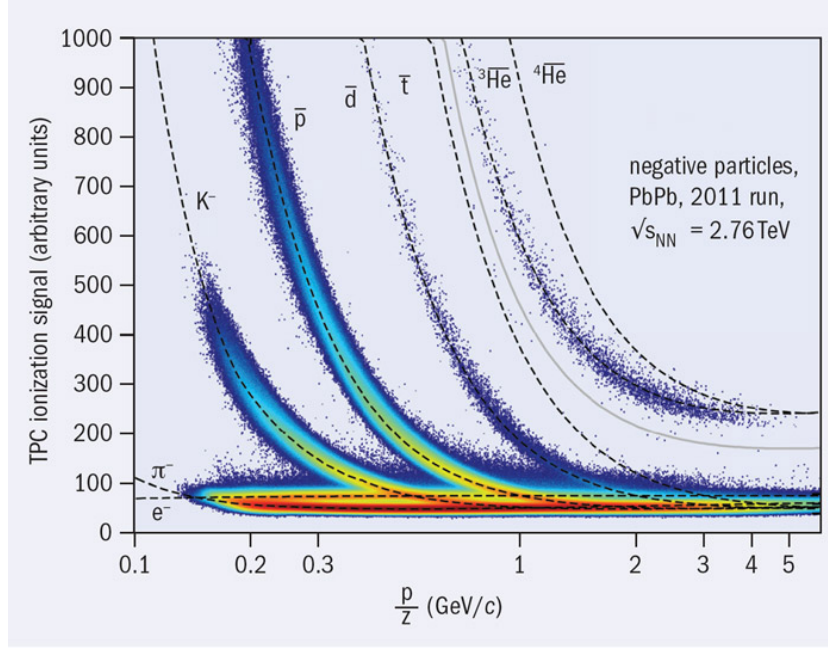


Figure 2.7: Ionization signals versus particle momentum for Pb-Pb collisions in ALICE. Dashed lines show curves defined by the Bethe-Bloch formula 2.1 [21]

Given that the momentum of the particle is required for correlating the energy loss signal to particle species, our outreach detector cannot explicitly do PID measurements. Still, looking at the energy loss signal and using some assumptions about the types of particles we expect to measure with our detector (minimum-ionizing cosmic tracks and highly-ionizing decay products), the outreach chamber will be able to showcase the difference between different types of particles via their energy loss signal.

2.2 Readout System

The signal induced in the induction gap by the amplified electrons can be measured as a small, negative analog signal. That signal is first amplified further and then digitized by a comparator in a work done by Oguz Duran, who wrote his bachelor's thesis on the subject [22]. A quick overview of his work will be given before elaborating on the final circuit board which was this thesis' main effort to complete the read-out system.

2.2.1 Negative Gain Amplifier

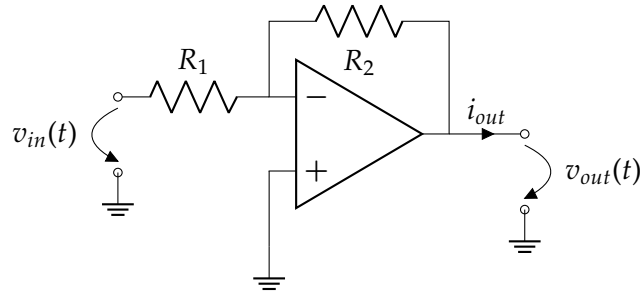


Figure 2.8: Amplifier with negative gain $= -\frac{R_2}{R_1}$. [22]

Figure 2.8 shows a simple operational amplifier (OPAMP), an electronic component with high gains. This negative feedback amplifier inverts the electron-induced signal to be positive compared to ground. The SN10501DBVT by Texas Instruments was chosen and can multiply input signals by a factor of over 30. The signal after amplification is shown in figure 2.9. The signal's shape is still the same as the induction pattern produced at the anode.

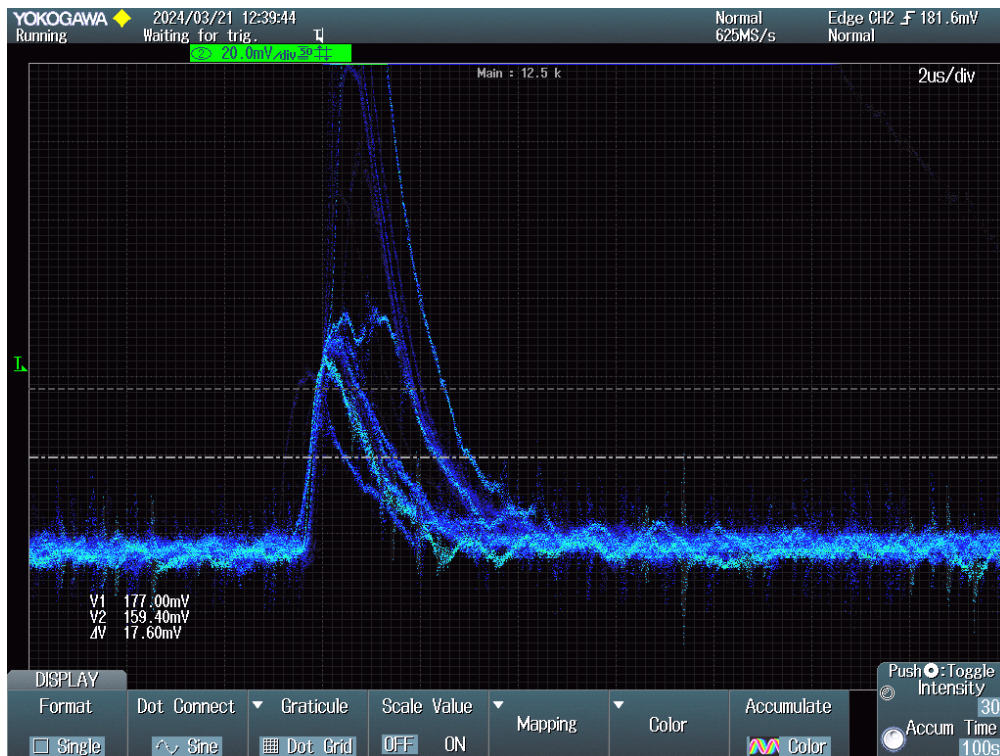


Figure 2.9: Oscilloscope plot of the output waveform (tones of blue) collected over a few seconds. We see the proper induction pattern produced by the GEM chamber anode.

The final circuit board features multiple capacitors parallel to the DC power supply

to filter out high frequency noise. While an ideal OPAMP has infinite gain and no signal offset, the reality is different. The incurred DC load was overcome by adding a DC-blocking capacitor.

2.2.2 Comparator

A comparator is a one bit Analog Digital Converter (ADC), comparing two voltages and outputting a signal based on the result of the comparison. The MCP6561RT-E/OT analog comparator by Microchip Technology was chosen for its low cost and because it can handle the short signals (order of $1\ \mu\text{s}$) coming from the amplifier, which are too fast for some other comparators to handle. By default the comparator emits a ground signal. If the signal from the negative gain amplifier exceeds a set threshold a 5 V signal is emitted for the duration of the signal above the threshold. This time is called time-over-threshold (ToT). This time is crucial as it retains information about the peak amplitude. Figure 2.10 demonstrates how stronger signals result in longer ToT. This way we can still infer the number of ionizations by the initial particle from the square-wave output signal of the comparator, shown in figure 2.11. The length of the comparator signal corresponds to the ToT.

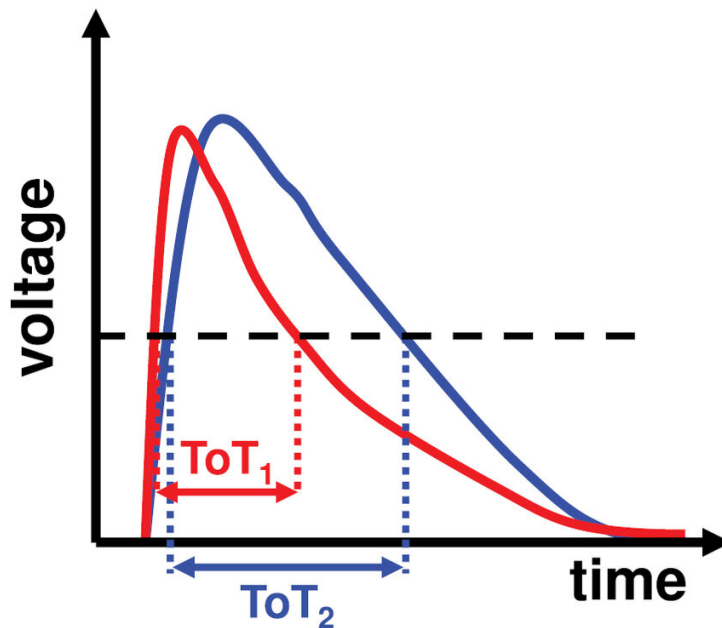


Figure 2.10: Illustration of time-over-threshold for pulse shape discrimination. [23]

2 GEM based demonstrator

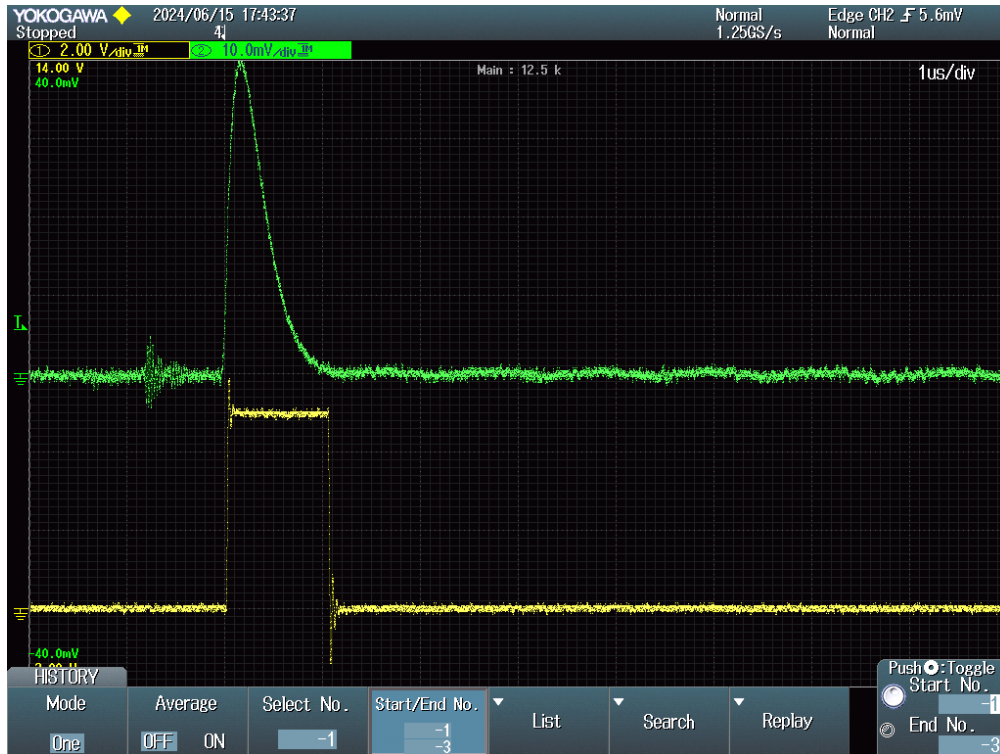


Figure 2.11: Oscilloscope plot of the output (yellow) waveform of the comparator in comparison to the input (green) waveform produced by the amplifier stage before. A measurable phase delay is present, as well as a small back EMF-caused signal to noise at the input when the comparator outputs.

2.2.3 Interlude

When work for this thesis began the detector's electronics was developed to this point. Initial measurements to familiarize myself with the setup has shown unexpected behaviour. After a lot of trial and error two faults were identified. The setup was not connected to a stable power source and an uninsulated wire inside the drift volume was constantly ionizing the gas. The detector has been moved to a stable power source and the gas chamber was opened to insulate the wire. Fearing the output was too chaotic we were willing to give up on the information of the signal's strength and developed a circuit, schematic shown in figure 2.12, for a binary 'hit' or 'no hit' read-out.

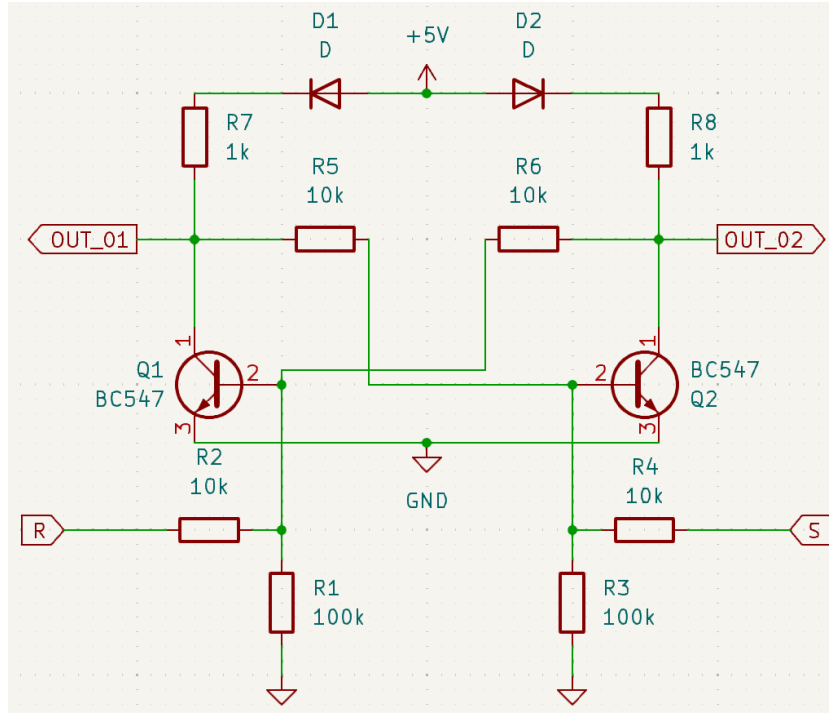


Figure 2.12: Schematic of an SR latch, also known as a flip-flop, is a circuit with two stable states. They are used as data storage elements.

A SR latch has two stable states, one is on by default. We interpret that state as 'no hit'. An arriving signal would be sent to the base of one transistor, causing the circuit to flip states to 'hit'. When the hit has been registered a small pulse to the base of the other transistor causes the state of the circuit to 'flop' back to its default state. Hence these circuits are sometimes called flip-flops. This circuit has been tested on a breadboard and would work. Fortunately the above described faults could be resolved and a circuit keeping proportionality information could be developed.

2.2.4 ToT signal to voltage converter

The final card was designed as part of this thesis. Its purpose is to convert the ToT to a voltage and store that voltage until read out. The idea is that the detector spends most of its time in integration mode, waiting for a signal to arrive. A signal arriving on a pad anytime during that period first gets amplified, converted into a digital time-over-threshold signal by the comparator and then that time is encoded as a voltage. Periodically these voltages are read out to be interpreted as a signal and are reset back to ground, ready and waiting for the next signal to arrive. In practice the comparator signal is used to charge a capacitor. To understand how a capacitor is charged, let's look at a simple circuit where a capacitor of capacitance C and a resistor of value R are connected in series, called a RC circuit and depicted in figure 2.13. Switch S can either be used to close the circuit with a voltage U_0 or short-circuit the RC circuit. Connecting the electrical source starts the switch-on process of the RC circuit and allows a current I to flow, charging the capacitor. For the purposes of Kirchhoff's second law the source

2 GEM based demonstrator

voltage has to be treated as negative $U_0 = -|U_0|$, giving the following equation:

$$U_0 + U_R(t) + U_C(t) = 0, \quad (2.15)$$

where $U_R(t) = R \cdot I(t)$ and $U_C(t) = \frac{Q(t)}{C}$ are the voltage drop across the resistor and the capacitor respectively and $Q(t)$ is the charge on the capacitor during the switch-on process. Substituting into Kirchoff's law, writing $I(t)$ as $\dot{Q}(t)$ and $U_0 = -|U_0|$, and a bit of rearranging we get this inhomogeneous differential equation of the 1st order

$$\dot{Q}(t) + \frac{1}{RC} \cdot Q(t) = \frac{|U_0|}{R} \quad (2.16)$$

with an initial condition of $Q(0) = 0$ for the charge of the capacitor. The function

$$Q(t) = C \cdot |U_0| \cdot \left(1 - e^{-\frac{t}{RC}}\right) \quad (2.17)$$

solves this differential equation and gives the quantity $\tau = RC$, called the RC time constant. Inserting the RC time constant into eq. 2.17 shows that τ is the time required for the charge to rise to

$$Q(\tau) = Q(RC) = C \cdot |U_0| \cdot \left(1 - e^{-\frac{RC}{RC}}\right) = C \cdot |U_0| \cdot \left(1 - \frac{1}{e}\right) \approx 63\% \cdot C|U_0|, \quad (2.18)$$

approximately 63% of its maximum. Now it is easy to find $U_C(t) = \frac{Q(t)}{C}$ as

$$U_C(t) = |U_0| \left(1 - e^{-\frac{t}{RC}}\right), \quad (2.19)$$

the function describing the voltage across the capacitor with respect to time. In theory the output signal from the comparator card could now be sent to such a RC circuit and charge a capacitor. Measuring the voltage across the Capacitor U_C we can then calculate what the ToT was that charged the capacitor by solving 2.19 for t :

$$t = RC \left(\log \left(\frac{U_0}{U_0 - V_C} \right) \right) \quad (2.20)$$

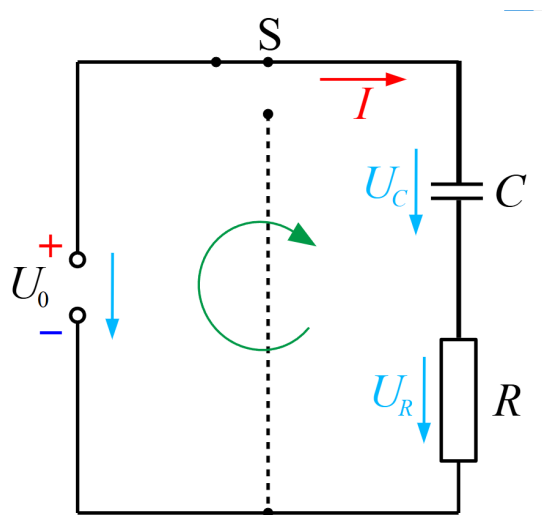


Figure 2.13: A diagram of a simple RC circuit. [24]

In reality the capacitor immediately starts discharging as soon as the comparator starts sending ground. The voltage across the capacitor would have to be measured at the instant the comparator signal ends or a wrong ToT and thus ionization signal would be inferred. Instead we would like for an incoming signal to charge the capacitor and for the capacitor to then keep that charge until U_C was measured. This is achieved using a bipolar junction transistor.

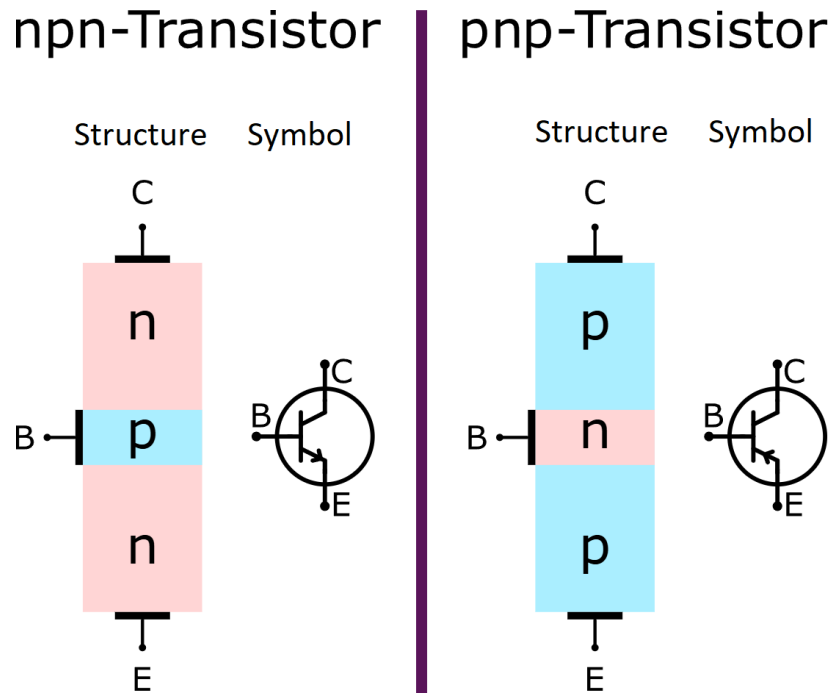


Figure 2.14: Schematic representation of a npn (left) and pnp (right) transistor structure and symbol in circuit diagrams [25]

A bipolar junction transistor consists of three alternating p- and n-doped semiconductor layers. The three layers are called collector (C), base (B) in the middle, and emitter (E). Depending on the doping sequence within the structure, a distinction is made between npn (negative-positive-negative) and pnp (positive-negative-positive) transistors. P-doped regions include impurities that provide electron holes and impurities in n-doped regions provide electrons. Both electrons and holes are used as charge carriers in the transistor. At the boundary between the two semiconductor materials, the depletion region, free electrons from the n-doped region fill available holes. This allows current to flow in one direction (forward direction, from p-type to n-type) with ideally no resistance while having ideally infinite resistance in the other (reverse direction). A single such connection is a diode. Real diodes can suffer breakdown if a large bias voltage is applied in reverse direction, permanently damaging the diode. While a smaller reverse bias is applied a small current can flow, as the resistance is not really infinite. In contrast to diodes a transistor has not one but two p-n junctions. It is therefore possible to understand a transistor as two diodes next to one another facing in opposite directions. In the npn-transistor both forward directions face away from the base and both face toward the base in the case of a pnp-transistor. Let's examine

the function of npn-transistors, the type used in the designed circuit board, more closely. Connecting collector and emitter to a circuit with a positive voltage lower than breakdown voltage across collector and emitter, a small current flows across the diode. We say the collector-base-diode is reverse biased and the base-emitter-diode is forward biased. Applying a small voltage across base and emitter allows the base-emitter junction to become conductive. Holes are injected into the emitter region from the base and electrons from the emitter into the base, allowing both to recombine. Having the emitter be doped more heavily than the base lets the flow of electrons dominate over that of the holes, resulting in a diffusion current through the base. Because the base layer is very thin, thinner than the diffusion length of the electrons, and is only lightly doped, recombination is unlikely and the majority (>99%) of electrons can diffuse into the collector-base junction. From there the electric field carries them into the collector, operating the collector-base diode in reverse direction.

In conclusion, a small current at the base nearly instantaneously allows a current to flow from collector to emitter. Cutting off the current to the base does not stop the above described process immediately, because the base voltage is only set to ground, not negative. A negative signal would put the base-emitter junction in reverse bias leading to an immediate cut-off. The delay increases if the base current provided more electrons than necessary for drift current to occur. This delay is not a huge problem, as the forward bias is set to zero anyways and the system reaches equilibrium on its own. The small noise at the falling edge of the comparator seen in figure 2.11, bemoaned by Oguz Duran [22], might help us here with the cut-off process. In any case, the ToT should not be calculated from the voltage measured at the capacitor according to formula 2.20, but should be calibrated with digital signals of known length in order to adapt it to the resulting voltage at the capacitors. This should be done for each channel individually, but due such a calibration has not been obtained for the readout channels of the outreach detector yet. However, the method for calibration and the formula for the fit are provided. A voltage divider is added between the comparator output and transistor base to decrease the current and avoid the issue described concerning the delay during the cut-off process. For the ToT the transistor sends a constant 5 V signal to a RC circuit. Now that the capacitor keeps its charge we have to discharge it ourselves after we have measured. Another transistor is added, acting like the switch in figure 2.13. The diagram shows the default state. If a signal is sent to the base of this second transistor, the capacitor can discharge freely. The Voltage for the discharge process is described by the time dependent function

$$U_C(t) = |U_0| \cdot e^{-\frac{t}{RC}}, \quad (2.21)$$

which satisfies the differential equation 2.16. This concludes the description of the circuit for one channel. The schematic done with KiCad software is shown in figure 2.15.

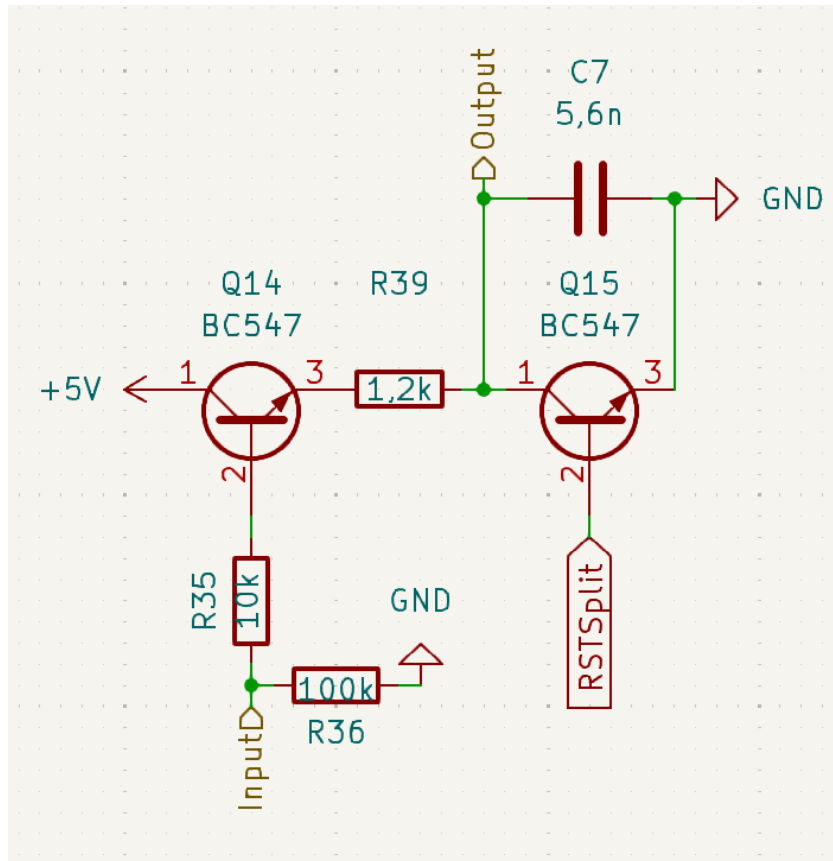


Figure 2.15: KiCad Schematic for one Channel. A RC circuit with a time constant $\tau = 6.72 \mu\text{s}$ was chosen.

The schematics are labeled ToT Capacitor Sheet 0.7 in further schematics. The read-out of the capacitor voltage is done with an Arduino. Since an Arduino has limited channels but the anode has 64 pads we decided to make use of a multiplexer (mux). A mux is an electronics component that allows to select one of multiple input channels and forward it to one output. The CD4051B CMOS Single 8-Channel Analog Multiplexer was chosen. It requires 5 V on the VDD pin, -5 V on the VEE pin, ground on VSS and Inhibitor (INH) pins as well as either a high or low signal on the pins labeled A, B and C to target one of 8 channels. [26] CBA concatenated gives thus a binary number, with a low signal representing a 0 and a high signal a 1, between 0 and 7. And finally one pin for the output signal brings the total number of pins up to 16 per mux. One such multiplexer module is shown in figure 2.16.

2 GEM based demonstrator

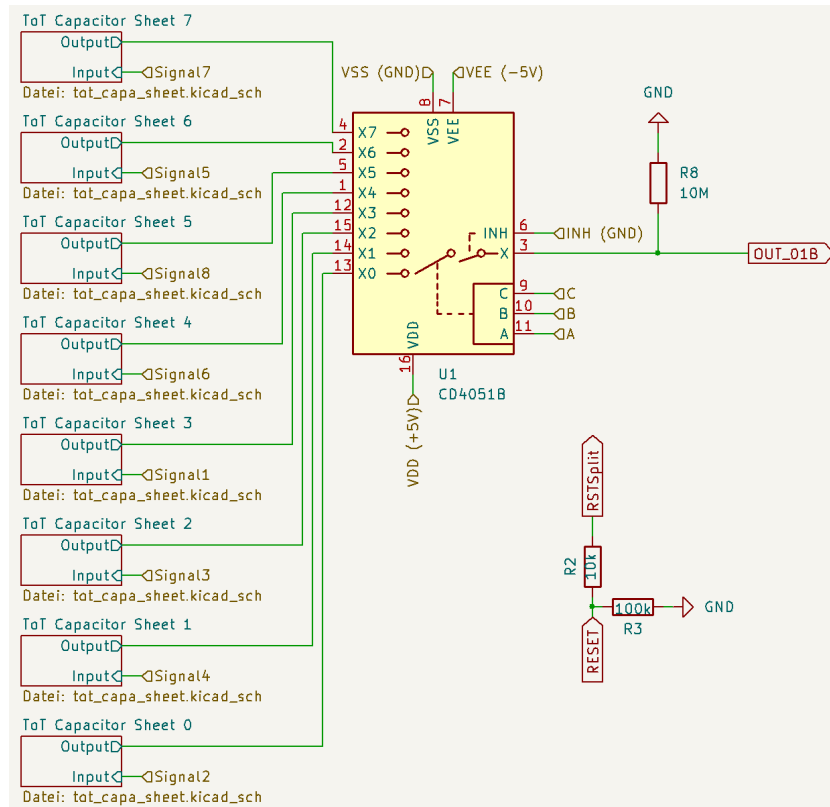


Figure 2.16: Schematic for one side of a PCB. The ToT Capacitor Sheets hide the circuit for one channel each. Resistance values for voltage dividers on output and reset signal are included. See appendix for the full schematic used in KiCad.

Two mux handling 16 channels in total are on a card, meaning 4 cards are needed to scan all 64 channels. The full schematic for a card is shown in the appendix 4.1 and 4.2. The PCB design from the schematic is shown in figure 2.17. Due to time constraints only one multiplexer module and the necessary circuitry to control the mux, meaning the voltage divider for the output signal and reset signal, as well as the pins to connect to other cards, have been soldered. This was enough to test every unique part of the card design. The code used for testing the cards is provided in the appendix 2. Further discussions will be made with regard to a pseudo code 1. Initial results suggest calibration will have to be done for each channel. Even without a signal, noise partially charges all capacitors over time. Over an integration period of 100 ms this typically results in a voltage below 0.15 V and can easily be filtered out with a single if-statement. Real signals would show up quite a bit larger, as will be discussed in the performance chapter. The code defines the modulus operandi of the detector. A cycle begins with an integration time of 100 ms. Any ionization event and resulting current on a pad during that period charges the corresponding capacitor. All channels of the mux are scanned and measured voltages are stored. Afterward the measurement circuit is reset by grounding all capacitors. 1 ms is dedicated to discharging the capacitors. Finally the measurement results are interpreted and can be displayed. The code controls one

2 GEM based demonstrator

mux handling eight channels. The reset and binary signal can be transmitted to all cards. Operation of all eight mux can be handled in tandem. The mapping of binary

```
double sensorValue_0 = 0;
...
double sensorValue_7 = 0;
void loop() {
    wait(100); //integration time
    for (int i=0, i<8, i++){
        sendABCSignal(i); //configure the mux, map int to channel
        sensorValue_i = readVoltage(); //save Voltages on capacitor for each channel
    }
    sendResetSignal(); //capacitors need about 1ms to discharge
    //calculations are done after resetting to keep dead Time short
    convertVoltageToSignalStrength([sensorValue_0, ..., sensorValue_7]);
    printResults();
}
```

Listing 1: Pseudo code for operating one mux. After an integration period all measurements are gathered and the System is reset, ready to collect new data.

number for the mux, meaning the A-, B-, C-Signals, to the input pins is a bit tricky and is thus listed in table. From top to bottom the pins are labeled 1F..8F, 1B..8B, depending on whether the pin is on the front (F) or back (B) side of the card. The keen observer notices from the PCB design, shown in figure 2.17, that there are ten pins on each side. That is because the middle two pins are to transmit ground between cards.

Pin	1F	2F	3F	4F	5F	6F	7F	8F	1B	2B	3B	4B	5B	6B	7B	8B
Mux	3	0	2	1	6	4	7	5	5	7	4	6	2	1	0	3

Table 2.2: Mapping between pins on the card and binary number needed for the mux to forward the signal from that pin.

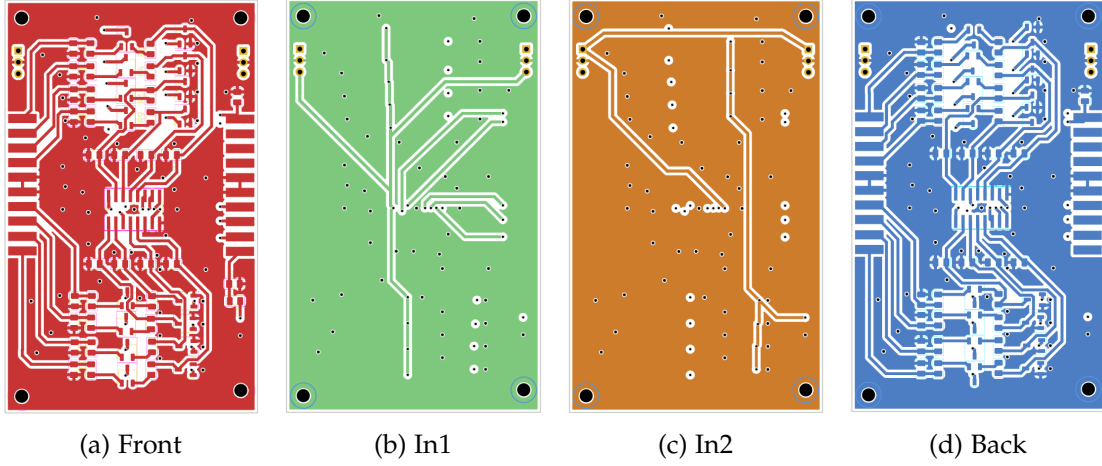


Figure 2.17: The four layers of the PCB as designed using KiCad.

The dead time of a detector is the period during which the detector is not sensitive to incoming events. For our detector this time is mainly due to the time required to ground the capacitors. A signal arriving at that moment would be lost. As can be seen in the code, this period lasts for 1 ms. The detector spends the rest and majority of the time during integration period. Should an ionizing event occur, then the resulting current on a given pad would charge up the corresponding capacitor. The capacitor is charged further, if another event occurs before read-out. This would distort the signal and lead to false interpretation. It would look like a particularly strong ionization event. If tracks are considered, a crossing of two paths would be visible with amplified signal strength in the cross section. The integration period is set to 100 ms. When measuring cosmic particles, about one event was detected every few seconds. To calculate the chance for multiple events to occur at once or to be lost to dead time, the following assumptions were made: Events are independent of one another. The chance for an event is constant. Events happen instantaneously. To justify the last premise a bit: A signal is typically on the order of 1 μ s, or 1000 times shorter than the dead time. With this scenarios where a signal might only be partially within one type of period are neglected. Let λ be the mean rate for one event to occur. The probability for observing no events in a time period t is given by the exponential function

$$P(0|\lambda) = e^{-\lambda t}, \quad (2.22)$$

which can be normalized to get the distribution

$$P(t) = \lambda e^{-\lambda t} \quad (2.23)$$

for the time t between events. Indeed, we are dealing with Poisson statistics. The probability for k events to occur in a time t is

$$P(k) = \frac{(\lambda t)^k e^{-\lambda t}}{k!} \quad (2.24)$$

With cosmics, assuming a rate of activity of $\lambda = 0.5$ s, we get a probability of $P(0) = 95.12\%$ from this equation for no event to occur in one cycle,

$$P(1) = \lambda t e^{-\lambda t} \approx 4.76\% \quad (2.25)$$

2 GEM based demonstrator

for one event and

$$P(> 1) = 1 - P(0) - P(1) < 0.12\% \quad (2.26)$$

for more than one event. From the ratio of dead time to total cycle time we get a below 1% chance for an event to fall into the detector's dead time. These numbers are quite satisfactory when measuring cosmics. If an active source is measured, the integration time may need to be adjusted.

2.3 Performance

The capacitor charge-up has been measured with an oscilloscope, result see figure 2.18, and shown to follow eq. 2.19 quite nicely.



Figure 2.18: Rising edge measurement done with an oscilloscope. The curve follows eq. 2.19 nicely.

To determine what RC constant τ to use tests with different values for τ and pulse lengths have been performed. Figure 2.19 shows the results of these tests. The measurements for pulse lengths of 500 ns and 5 μ s are particularly important, the expected times over threshold fall into that range. For optimal resolution we want the shorter time to be near the beginning of the exponential rise of the curve and the longer time near the end before the curve flattens out.

2 GEM based demonstrator

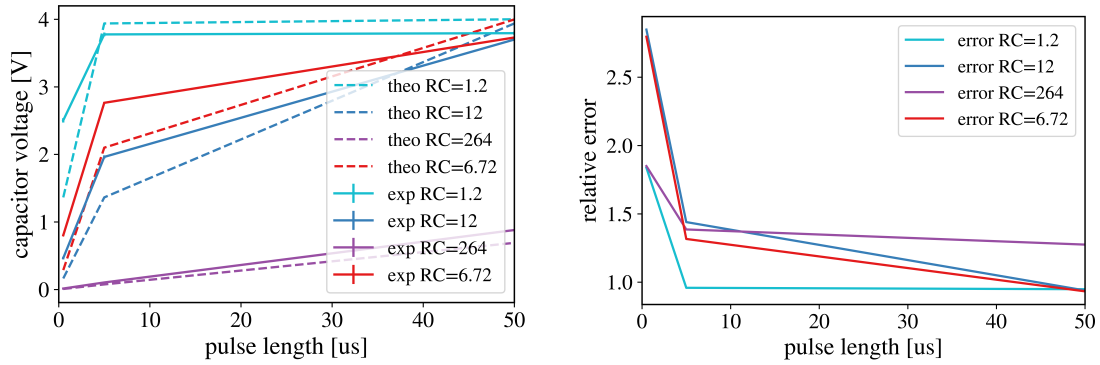


Figure 2.19: Left: Capacitor voltages versus pulse length for different RC values. Full lines for experimentally measured values, dashed for theoretical value using formula 2.19. Right: Ratio of measurement to theoretical value.

The RC constant with value $\tau = 1.2 \mu\text{s}$ should in theory be best, however even the shortest of signals already charged the capacitor to $\approx 63\%$ of its maximum in our tests. This would make it difficult to distinguish between larger signals. An RC constant with value $\tau = 12 \mu\text{s}$ puts short signals to the very beginning of the curve with the capacitors charged to about 12% of their maximum. But even a $5 \mu\text{s}$ signal, which is longer than any real signal we might expect, only charged the capacitor to about 49%, leaving a large part of the curve unused. A good middle ground is achieved with a value of $\tau = 6.72 \mu\text{s}$, using a $1.2 \text{ k}\Omega$ resistor and 5.6 nF capacitor. Now a short $0.5 \mu\text{s}$ signal charges the capacitor to $\approx 20\%$ and a long $5 \mu\text{s}$ signal to $\approx 69\%$, making good use of the full range available.

2 GEM based demonstrator

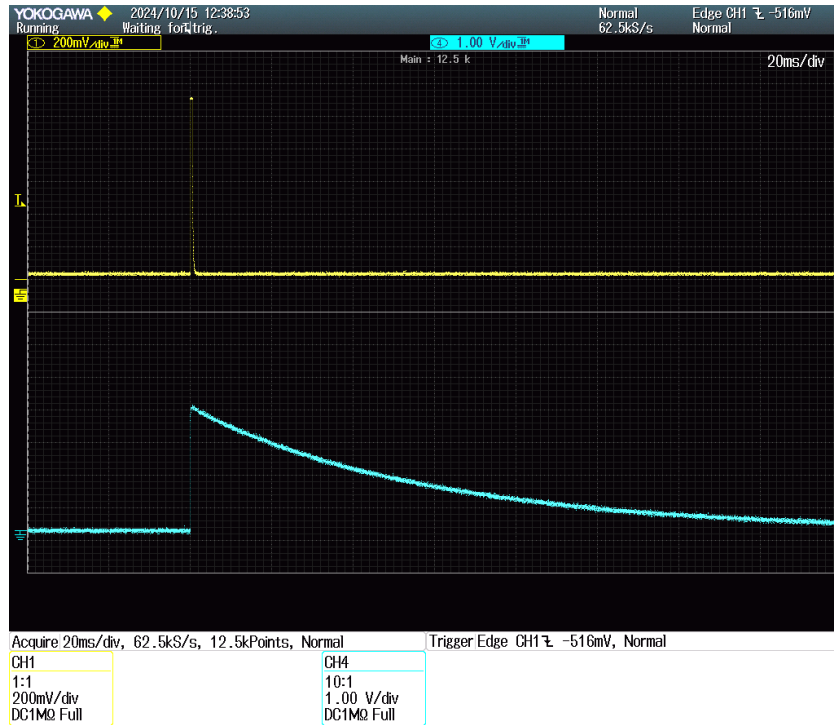


Figure 2.20: Falling edge measurement done with an oscilloscope. As with the rising edge measurement, the exponential curve is evident.

A measurement of the capacitor discharging recorded with an oscilloscope can be seen in figure 2.20. From this it might look like the time to reset (the dead time!) could last well over 100 ms. This is fortunately not the case. Connecting the oscilloscope messed with the RC constant of the circuit to change it to $\tau = 69$ ms. The discharge behaviour when a reset signal is applied has instead been explored with the Arduino. The Arduino is capable of measuring the voltage on the capacitor without any noticeable discharge. A time of 1 ms has proven reliable for discharging the capacitor to values around 0.05 V. Longer discharge periods suffer from greatly diminishing returns, due to the nature of exponential curves. A discharge all the way to ground would theoretically take infinite time.

2 GEM based demonstrator

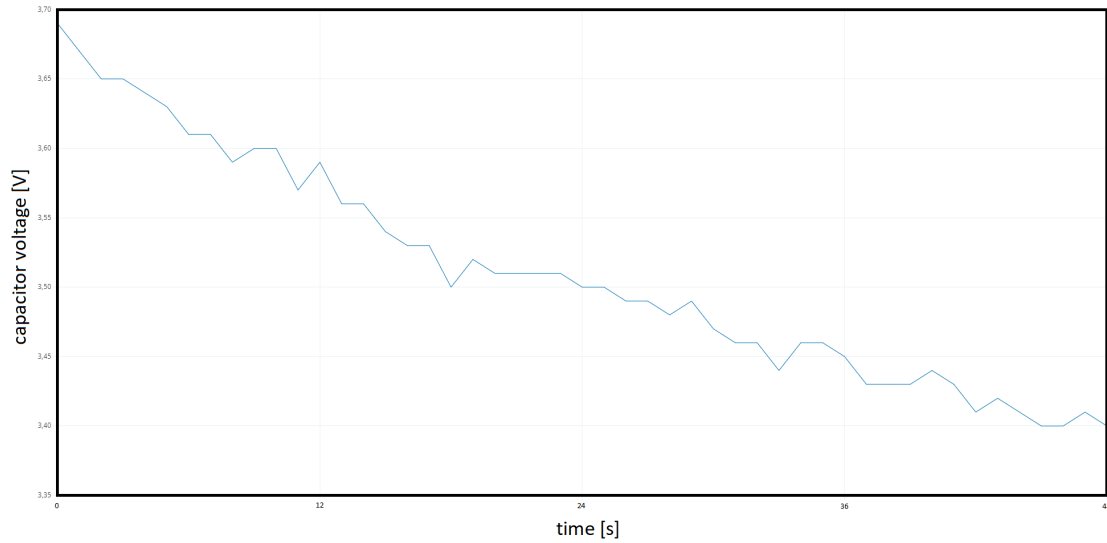


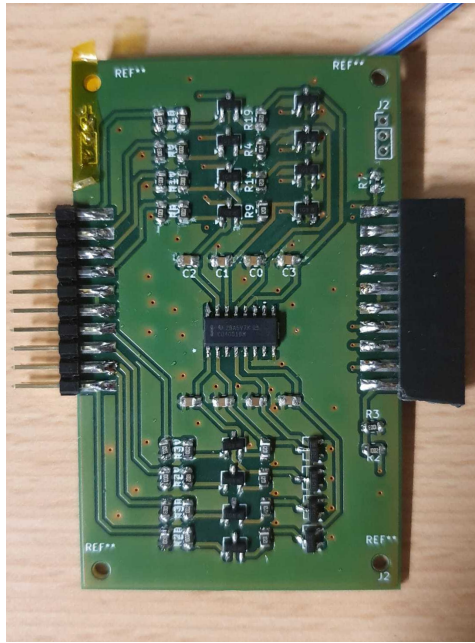
Figure 2.21: Voltage on a charged capacitor versus time. The voltage dropped off from 3.69 V to 3.40 V over 48 s.

Even without an applied reset signal the capacitor slowly discharges over time. It is not possible to measure this directly with an oscilloscope, as contact immediately starts actively discharging the capacitor. A plot 2.21 recorded with the Arduino shows the natural voltage drop off of the capacitor. The data shown is from the 'steep' part of the curve. Even here the average voltage drop is below 0.001 V/s. Since real signals typically fall lower on the curve, where the capacitor can keep the voltage for longer and readout happens every 0.1 s the voltage on the capacitor during operation can be considered constant.

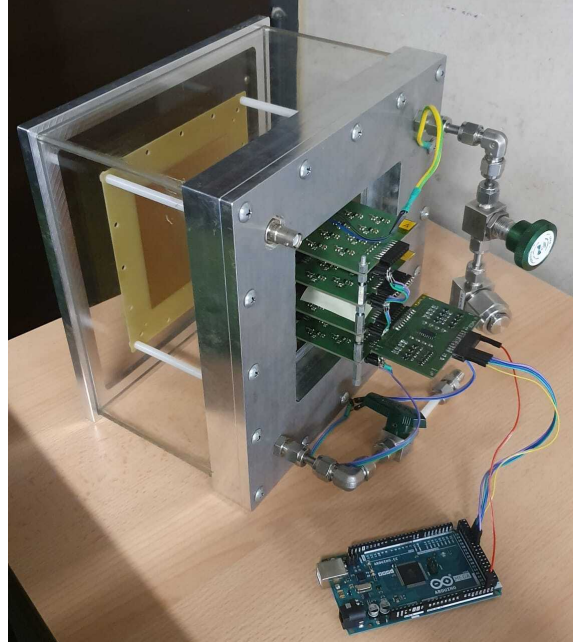
3 Summary, Conclusion and Outlook

3.1 Summary

In this thesis the theoretical background for the underlying phenomena at play in the operation and functionality of GEM based detectors has been explored. We first looked at ionization, the different reactions that lead to it and the accompanying phenomena of recombination and electron capture by CO_2 . We learned how in strong electrical fields one ionization can lead to another, causing the formation of electron avalanches. These avalanches are brought about by strong electrical fields in the holes of GEM electrodes. Following the explanation of the natural phenomena we explained signal shaping and the functionality of different electrical components responsible for them. Negative Gain Amplifiers boost signal strength and capacitors filter out high frequency noise. A comparator digitizes the analog signal. The length of the square-wave signal equals the time that the analog signals spends above a threshold. A transistor allows for a lower voltage to control a higher one using doped semiconductors. This is used to charge a capacitor. The capacitor's voltage corresponds to the time over threshold and thus the signal strength. The RC value τ dictates the behaviour for charging and discharging capacitors. A circuit has been designed to translate the ToT to a voltage stored on a capacitor, which can be reset. From the circuit schematic a PCB has been designed which also enables the readout of multiple channels via a single data line using a multiplexer. An eight channel module of the PCB has been soldered and controlled using an Arduino. The assembled card can be seen in figure 3.1a, the outreach chamber with the new card and the Arduino operating the electronics are shown in 3.1b. Preliminary measurements show the designed card works as desired. Probability theory has been considered in the Arduino code to minimize chances for erroneous measurement results, where a detection efficiency of 99% is expected to be reached for cosmic tracks with the outreach detector.



(a) The produced readout board for converting the multichannel ToT signal from the comparator card to an analog signal which can be readout with an Arduino.



(b) Photo of the produced readout board plugged into the outreach chamber and the Arduino Mega responsible for the data taking.

Figure 3.1: Readout Board and Outreach Chamber Setup

3.2 Conclusion

Working on this project taught me many things. I got to experience working for a project that was already in full swing with a team, exercising proper lab etiquette. Trying to understand the work done before me taught me to interpret circuit board designs. Fitting in to an ongoing project I developed schematics to suit the application purposes and create PCB designs from a schematic using the software KiCad. Hands-on experience has once again proven to be highly effective for learning, in my case learning a lot about electronics and the myriad of components. I learned the hard way to spot errors in PCBs and the importance of proper time management for a project. I have soldered for the first time and quickly improved. Writing the thesis I learned how to search for scientific sources and how to cite them appropriately.

3.3 Outlook

Due to time constraints the project could not be finished entirely. The method for calibration has been presented. The calibration itself is then straight-forward. The rest of the cards still needs to be soldered. This is just a matter of repeating what has already been done and proven to work. As an aspiring teacher I intend to continue being involved with the project. A pilot run is planned for this semester. For that pilot run I

3 Summary, Conclusion and Outlook

intend to guide the students in their use of the detector. I will explain its constituent systems and how to safely operate the detector. Being prepared to answer the students questions, helping them interpret their results and assisting them as needed will be my job both for this project and in the future as a teacher. Beyond the knowledge that lies on the surface, the students will learn to become competent working in laboratory conditions, how to take notes in a manner that will be useful to them in the future and to accurately describe the experimental setup and results. Finishing the menial tasks of calibration and soldering as soon as possible goes without saying. I would love to be there and help guide the pupils to first explore all that Origins Go-To School will have to offer.

4 Appendix

```
// Pins A-, B- and C-Signal to Multiplex
const int APin = 35;
const int BPin = 33;
const int CPin = 31;
const int Pulse = 27;
// Pin for Reset Signal
const int RPin = 29;
// Pin for the Signal / Measurement
const int SPin = A14;
double sensorValue = 0;
#define GET_BIT(x, i) (((x) >> (i)) & 1)void setup() {
  pinMode(SPIn, INPUT);
  pinMode(APin, OUTPUT);
  pinMode(BPin, OUTPUT);
  pinMode(CPin, OUTPUT);
  pinMode(RPin, OUTPUT);
  pinMode(Pulse, OUTPUT);

  digitalWrite(APin, LOW);
  digitalWrite(BPin, LOW);
  digitalWrite(CPin, LOW);
  digitalWrite(Pulse, LOW);
  digitalWrite(RPin, LOW);
  Serial.begin(9600);
}
```

4 Appendix

```
void loop() {
  for(int chID=0; chID<8; chID++){
    digitalWrite(APin, GET_BIT(chID,0u));
    digitalWrite(BPin, GET_BIT(chID,1u));
    digitalWrite(CPin, GET_BIT(chID,2u));
    delay(0.1);
    sensorValue = analogRead(SPin)*(5.0 / 1023.0);
    //Serial.print("\n");
    //Serial.print(chID);
    //Serial.print(": ");
    //Serial.print(sensorValue*(5.0 / 1023.0));
    if(sensorValue > 0.15) {
      Serial.print("\n Hit on: ");
      Serial.print(chID);
      Serial.print("\n Amplitude: ");
      Serial.print(sensorValue);
    }
  }
  //resetting capacitors results in dead time
  digitalWrite(RPin, HIGH);
  delay(1);
  digitalWrite(RPin, LOW);
  //integration time
  delay(100);
}
```

Listing 2: Code for multi-channel read-out. Commented out code gives exact voltage read, code block below is a binary 'hit' or 'no hit' mode. These are to be replaced with a function generated from sensor calibration to give a value for ToT, representing initial ionisation signal strength.

4 Appendix

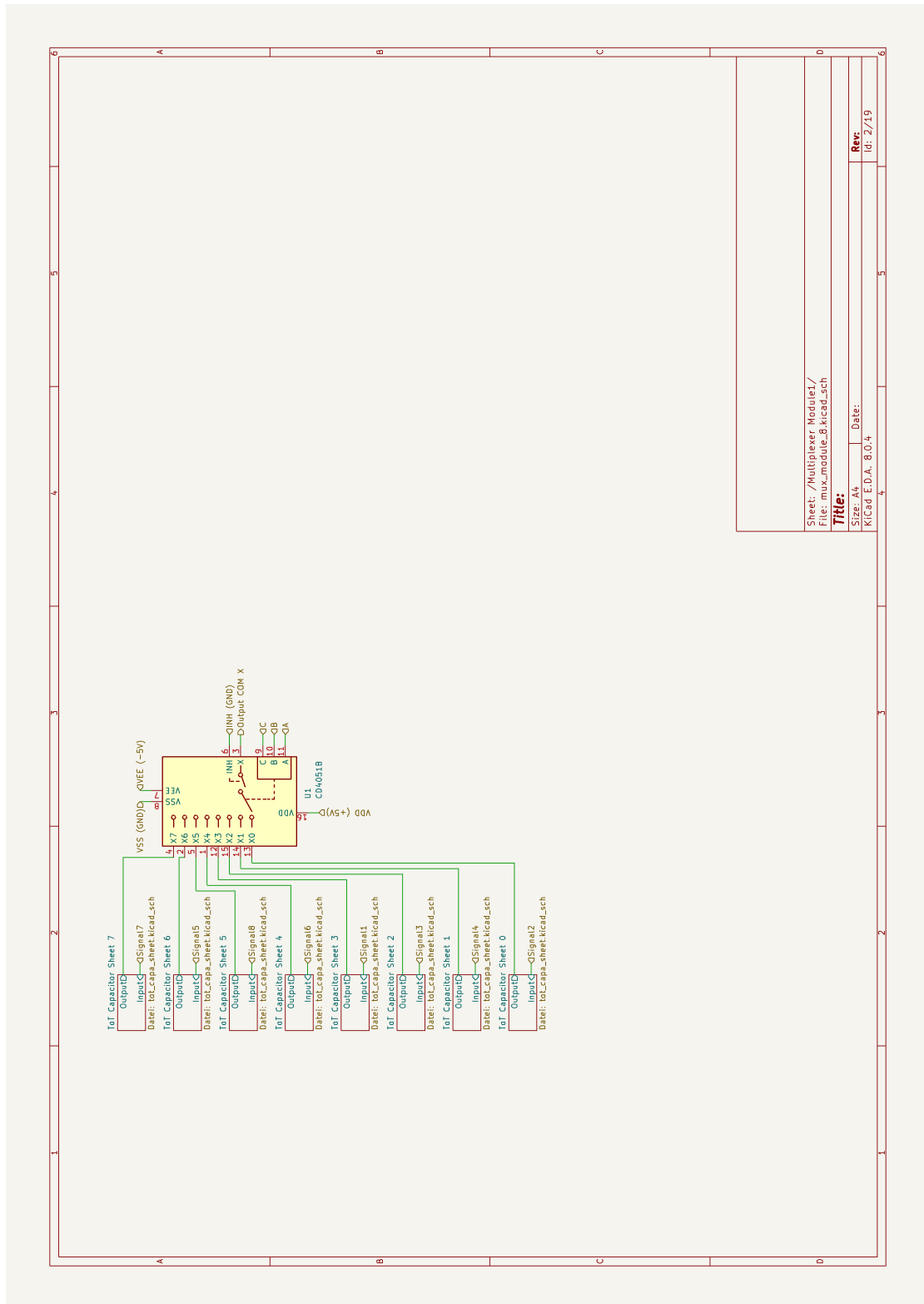


Figure 4.1: Schematic for a multiplexer module used in KiCad.

4 Appendix

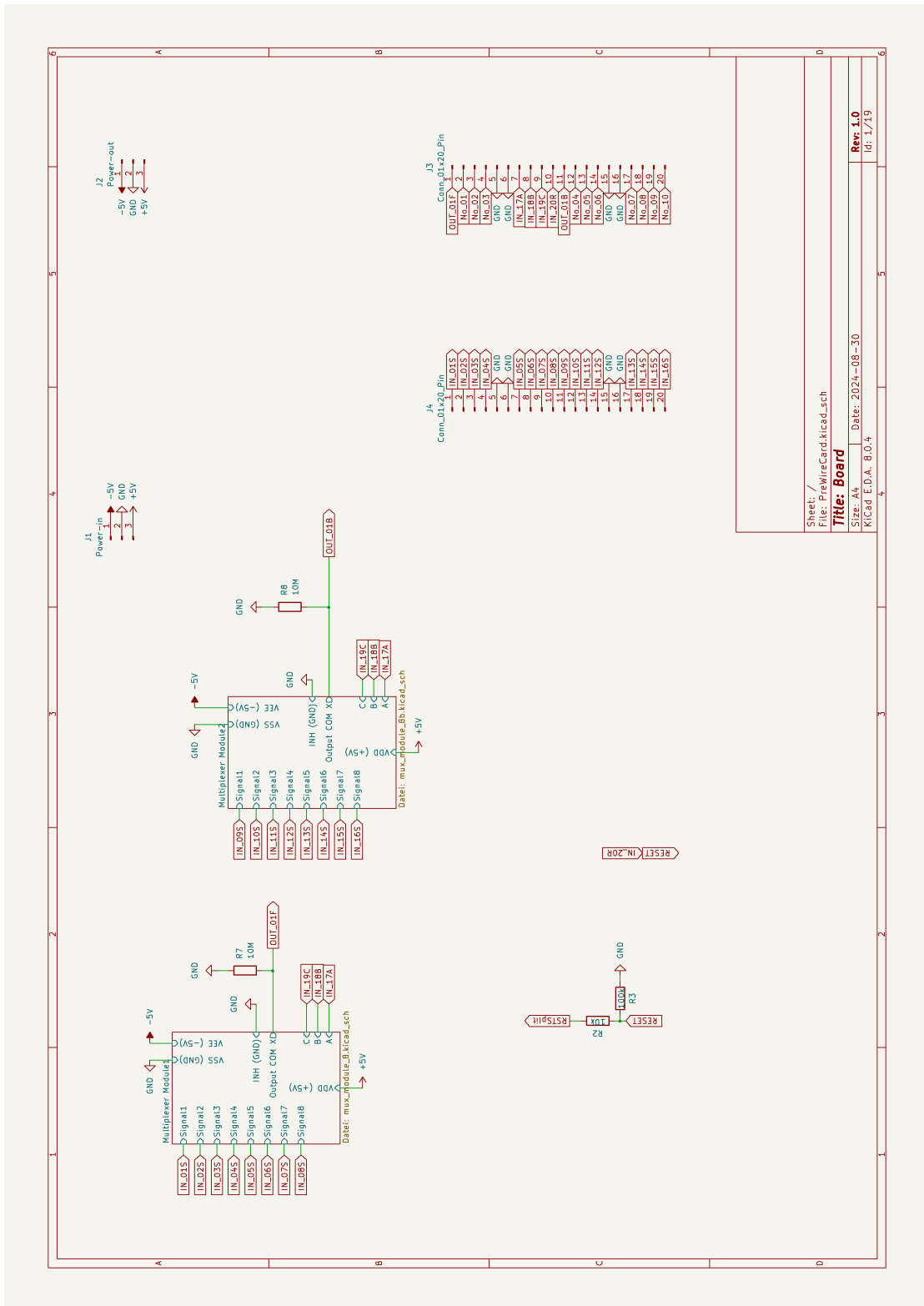


Figure 4.2: Schematic for the full circuit

Acknowledgments

Thank you to professor Fabietti for giving me the opportunity to be part of this wonderful project on such short notice. Leonardo Burgia has been invaluable in introducing me to the laboratory and providing insights into the status of the detector in the beginning. My uncle is an Arduino enthusiast and has infected me as well. Hearing about the subject for my thesis for the first time, he immediately offered me a simple temperature and humidity sensor and an Arduino to allow me to familiarize myself with the topic. I would like to express my gratitude to my friends and family for their unwavering support during this journey. A special thanks to Berkin Ulukutlu for his endless patience and for being there to support me at every step.

List of Figures

1.1	Picture of the CERN Minipix detector. [5]	2
1.2	Photo of the Lego model, to be built by the students to learn the different detector systems of the ALICE experiment.	3
2.1	GEM Detector Render and Outreach Chamber Photo	5
2.2	Number of ions collected versus the voltage for a singular wire ionization detector for α and β particles. [15]	7
2.3	Product of momentum transfer cross section and fractional concentration by volume, F , versus electron energy for pure CO ₂ and a 95/5 argon/CO ₂ gas mixture. Elastic scatters on argon dominate at higher energies. The Ramsauer minimum can be seen. [16]	9
2.4	Drift Velocity and Transversal Diffusion of Ar/CO ₂ Mixtures	10
2.5	Electron attachment coefficients as a function of field E for various Ar/CO ₂ mixtures at 1 bar. The process considered is 2.12 [16]	11
2.7	Ionization signals versus particle momentum for Pb-Pb collisions in ALICE. Dashed lines show curves defined by the Bethe-Bloch formula 2.1 [21]	14
2.8	Amplifier with negative gain = $-\frac{R_2}{R_1}$. [22]	15
2.9	Oscilloscope plot of the output waveform (tones of blue) collected over a few seconds. We see the proper induction pattern produced by the GEM chamber anode.	15
2.10	Illustration of time-over-threshold for pulse shape discrimination. [23]	16
2.11	Oscilloscope plot of the output (yellow) waveform of the comparator in comparison to the input (green) waveform produced by the amplifier stage before. A measurable phase delay is present, as well as a small back EMF-caused signal to noise at the input when the comparator outputs.	17
2.12	Schematic of an SR latch, also known as a flip-flop, is a circuit with two stable states. They are used as data storage elements.	18
2.13	A diagram of a simple RC circuit. [24]	19
2.14	Schematic representation of a npn (left) and pnp (right) transistor structure and symbol in circuit diagrams [25]	20
2.15	KiCad Schematic for one Channel. A RC circuit with a time constant $\tau = 6.72 \mu\text{s}$ was chosen.	22
2.16	Schematic for one side of a PCB. The ToT Capacitor Sheets hide the circuit for one channel each. Resistance values for voltage dividers on output and reset signal are included. See appendix for the full schematic used in KiCad.	23
2.17	The four layers of the PCB as designed using KiCad.	25

List of Figures

2.18	Rising edge measurement done with an oscilloscope. The curve follows eq. 2.19 nicely.	26
2.19	Left: Capacitor voltages versus pulse length for different RC values. Full lines for experimentally measured values, dashed for theoretical value using formula 2.19. Right: Ratio of measurement to theoretical value.	27
2.20	Falling edge measurement done with an oscilloscope. As with the rising edge measurement, the exponential curve is evident.	28
2.21	Voltage on a charged capacitor versus time. The voltage dropped off from 3.69 V to 3.40 V over 48 s.	29
3.1	Readout Board and Outreach Chamber Setup	31
4.1	Schematic for a multiplexer module used in KiCad.	35
4.2	Schematic for the full circuit	36

List of Tables

2.1	Energy levels of Argon [18].	11
2.2	Mapping between pins on the card and binary number needed for the mux to forward the signal from that pin.	24

Bibliography

- [1] Kultusministerkonferenz (KMK). Erkenntnisgewinnungskompetenz der Bildungsstandards. Bildungsstandards für die Allgemeine Hochschulreife, Accessed: 2024-10-18. 2020.
- [2] Nebelkammer: Aufbau und Funktionsweise. Accessed: 2024-10-18. 2024. URL: https://www.desy.de/sites2009/site_www-desy/content/e219828/e245574/e245601/e258642/e262691/e262763/e306517/Nebelkammer_ger.pdf.
- [3] Outreach award initiative to teach high school physics with CERN detectors. Accessed: 2024-10-18. 2022. URL: <https://home.cern/news/news/knowledge-sharing/outreach-award-initiative-teach-high-school-physics-cern-detectors>.
- [4] Timepix-based detectors bring particle physics into the classroom. Accessed: 2024-10-18. 2021. URL: <https://kt.cern/news/news/knowledge-sharing/timepix-based-detectors-bring-particle-physics-classroom>.
- [5] CERN-PHOTO-201910-356-1: Image from CERN. Accessed: 2024-10-18. 2019. URL: <https://cds.cern.ch/images/CERN-PHOTO-201910-356-1>.
- [6] Lehrplan für das bayerische Gymnasium (8. Klasse). Accessed: 2024-10-18. 2023. URL: https://www.gym8-lehrplan.bayern.de/contentserv/3.1.neu/g8.de/id_27338.html.
- [7] Fachlehrplan Physik für das bayerische Gymnasium (8. Klasse). Accessed: 2024-10-18. 2023. URL: <https://www.lehrplanplus.bayern.de/fachlehrplan/gymnasium/8/physik>.
- [8] MuonPi interactive map. Accessed: 2024-10-18. 2024. URL: <https://muonpi.org/interactive-map.html>.
- [9] MuonPi mission statement. Accessed: 2024-10-18. 2024. URL: <https://muonpi.org/our-mission.html>.
- [10] How do I get a detector? Accessed: 2024-10-18. 2024. URL: https://wiki.muonpi.org/index.php?title=How_do_I_get_a_detector.
- [11] ALICE LEGO Model Assembly Guide. Accessed: 2024-10-18. 2024. URL: https://drive.google.com/file/d/1pi8m4h9IcMcfJGV2NundZLaV_8whfKrW/view?pli=1.
- [12] Gas Electron Multiplier (GEM). Accessed: 2024-10-18. 2023. URL: <https://cms.cern/detector/detecting-muons/gas-electron-multiplier>.
- [13] W. R. Leo. Techniques for nuclear and particle physics experiments: a how-to approach. Springer Science & Business Media, 2012.
- [14] Lab Manual: T08 - Techniques for Nuclear and Particle Physics. Accessed: 2024-10-18. 2022. URL: https://institut2a.physik.rwth-aachen.de/de/teaching/praktikum/Anleitungen/T08_20220218.pdf.

Bibliography

- [15] A. C. Melissinos and J. Napolitano. Experiments in Modern Physics. 2nd. Academic Press, 2003. ISBN: 978-0124898516.
- [16] D. M. Binnie. Drift and Diffusion of Electrons. Accessed: 2024-10-18. 1982. URL: https://inis.iaea.org/collection/NCLCollectionStore/_Public/15/073/15073101.pdf.
- [17] F. Sauli. "Transport Properties of Gases and Gas Mixtures for Detectors". In: Nuclear Instruments and Methods in Physics Research A 386 (1997), pp. 531–534. DOI: 10.1016/S0168-9002(96)01172-8.
- [18] T. Argus and P. Oed. "Quenching of Photons in Argon-CO Proportional Counters". In: Nuclear Instruments and Methods in Physics Research A 233 (1985), pp. 114–118. DOI: 10.1016/0168-9002(85)90671-9.
- [19] F. Sauli and A. Sharma. "High-Precision Gas Gain and Energy Transfer Measurements in Ar-CO Mixtures". In: Nuclear Instruments and Methods in Physics Research A 350 (1994), pp. 230–234. DOI: 10.1016/0168-9002(94)91316-2.
- [20] GEM (Gas Electron Multiplier). Accessed: 2024-10-18. 2023. URL: <https://gdd.web.cern.ch/gem>.
- [21] Particle identification in ALICE boosts QGP studies. Accessed: 2024-10-18. 2023. URL: <https://cerncourier.com/a/particle-identification-in-alice-boosts-qgp-studies/>.
- [22] O. Duran. Bachelor Thesis: Design and construction of a gaseous detector readout system for use in. Accessed: 2024-10-18. 2024. URL: https://www.das.ktas.ph.tum.de/DasDocs/Public/Bachelor_Theses/BachelorThesis_OguzDuran.pdf.
- [23] Illustration of time-over-threshold (ToT) for pulse shape discrimination. Accessed: 2024-10-18. 2017. URL: https://www.researchgate.net/figure/Illustration-of-time-over-threshold-ToT-for-pulse-shape-discrimination_fig1_312465083.
- [24] Aufladen eines Kondensators (Theorie). Accessed: 2024-10-18. 2024. URL: <https://www.leifiphysik.de/elektrizitaetslehre/kondensator-kapazitaet/ausblick/aufladen-eines-kondensators-theorie>.
- [25] Transistor Formalitäten (Grundwissen). Accessed: 2024-10-18. 2024. URL: <https://www.leifiphysik.de/elektronik/transistor/grundwissen/transistor-formalitaeten>.
- [26] T. Instruments. CD4051B CMOS Single 8-Channel Analog Multiplexer/Demultiplexer Datasheet. Accessed: 2024-10-18. 2016. URL: <https://www.ti.com/lit/ds/symlink/cd4051b.pdf>.